Pergamon

Journal of Structural Geology, Vol. 16, No. 10, pp. 1463 to 1476, 1994

0191-8141/94 $7.00+0.00

0191-8141(94)E0005-J

Micro- and meso-scale deformation structures in experimental fault zones

K. K. CHATTERJEE

Geotechnical Laboratory, Geological Survey of India, Seminary Hills, Nagpur-440006, India

(*Received* 7 *December* 1992; *accepted in revised form* 20 *December* 1993)

Abstract—Kinematic structures of brittle, brittle–ductile and ductile shear zones were developed in experimental simple shear deformation. Transparent films of paraffin wax, with different initial fabrics, were progressively deformed in a manually-driven, stage-mounted shear-apparatus producing heterogeneous simple shear (γ = 0.36–2.64) at variable strain rates of from 3.3×10^{-5} to 4.08×10^{-5} s^{-1}. En échelon fracture arrays, compressive and tensile bridges, spaced cleavage, stylolite-like cleavage and sigmoidal cleavage trails were developed in brittle and brittle–ductile deformation. Structures produced in ductile experiments were *C′–S* and *C–S* fabrics, σ- and δ-type asymmetric tails, shear lenses and active folds of pre-existing and induced anisotropy planes. The experiments offer insight into the microstructural processes involved, and demonstrate development of a progression of shear structures in a single, non-steady deformation.

INTRODUCTION

THERE has been an increasing interest in recent years in the use of kinematic structures that reveal certain aspects of deformation in fault zones. In structural analysis of brittle fault zones, for instance, en échelon fracture arrays with associated bridges, and within-bridge microstructures provide shear- and sense-of-shear-criteria on all scales (Gammond 1983, 1987, Hancock 1985, Petit 1987). Similarly, a host of microstructures such as *C′–S* and *C–S* fabrics, σ- and δ-type asymmetric tails, shear lenses and stable and unstable folding of pre-existing and shear-induced planar fabric, has proved to be of kinematic significance in non-coaxial ductile deformation (Berthé *et al.* 1979, Berthé & Brun 1980, Ramsay 1980, White *et al.* 1980, Ghosh 1982, Lister & Williams 1983, Simpson 1983, Vernon *et al.* 1983, Lister & Snoke 1984, Casas 1986, Hanmer 1986, Ghosh & Sengupta 1987, and others).

While field and theoretical studies on the origin of shear zone structures are exhaustive, there are only a few analogue experiments that provide insight into the related grain-scale processes (Means & Xia 1981, Hobbs *et al.* 1982, Wilson 1984, Means 1989). The approach so far has been to simulate a single set of microstructures in pure shear or simple shear, and to study the related mechanisms of deformation. With such an approach, the range of shear zone micro-fabrics and structures that can develop with progressive deformation is only partly simulated. Moreover, in many natural shear zones, an array of structures develops progressively from a non-foliated, single-phase rock material with a geometrically isotropic fabric.

This paper describes the features associated with the development of experimental shear zones in a single-phase analogue material having an initial near-random fabric or locally non-random fabric. Using a manually-driven, stage-mounted shear-apparatus to induce progressive deformation in transparent films of paraffin wax, a spectrum of micro- and meso-scale structures was produced. The experiments reveal some aspects of microstructural processes associated with brittle, brittle–ductile and ductile shear zones.

EXPERIMENTAL SET-UP

Analogue material

Reagent grade paraffin wax (manufactured by Ranbaxy Laboratories, India, Ltd) has been used as the analogue material. Its low elastic and viscous yield strengths, strain-softening ability and temperature-dependent viscosity (Neurath & Smith 1982) are ideal, under the present experimental conditions, for shear instabilities to develop. Although the viscosity of paraffin wax is vastly different from most single-phase rock materials, its polycrystalline habits can be manipulated with heat treatment to simulate natural rock-fabrics. Complete physical and optical properties of paraffin wax may be found in Dunstan *et al.* (1938) and Jacoby (1976). It is relevant to note that paraffin wax melts incipiently along grain boundaries at 52–54°C. Its viscosity at 51°C is about 10^5 poise, and it strongly increases with falling temperature, a property useful in producing initial fabric anisotropy in the sample films (to be discussed later in this paper). Paraffin wax crystallizes in the orthorhombic system in plate and needle forms. In sample films about 30–40 μm thick paraffin crystals are transparent to translucent in plane-polarized light and give grey and yellow interference colours under crossed nicols. With increasing temperature, an irreversible transition takes place from plates to needles, a mode of recrystallization particularly useful in simulating progressive development of micro-fabric under strain.

Apparatus

To induce deformation, a manually-driven, stage-mounted shear-apparatus (Fig. 1a), similar in essentials to the assembly described in Means & Xia (1981), was used. The component parts of the set-up are as in Means (1989), except for the ramming device which comprises a guided screw with 40 turns per inch (or 0.625 mm per turn) attached to one end of the fixed base plate (Fig. 1b) holding the lower glass slide. The screw is manipulated with the fingers to propel the upper glass slide for ramming. 'Frosted grip' type 'propellers', ground one each on either glass slide of the assembly, have a clear space 5 mm across between them so that, with sandwiched films 45 mm long, an open-ended deformable zone of finite width and length is formed between rigid boundaries.

Experimental constraints

A single, non-steady but continuous deformation was imposed by left-lateral simple shear with the XZ principal plane of finite strain ($X \geq Y \geq Z$) lying horizontal and parallel to the sample plane, and the Y axis lying vertical and parallel to the microscope axis. For five brittle experiments, with each experiment run for 3 cumulative hours at temperature T = 0.90–0.91 T_m (where T is expressed as a fraction of melting temperature, T_m, of wax in Kelvins), displacements varied from 1.8 to 2.2 mm, giving a variation in shear strain, γ, of from 0.36 to 0.44. For five ductile experiments, with each experiment run at a temperature of T = 0.93–0.96 T_m for 18 cumulative hours, displacements varied from 10.75 to 13.22 mm, with γ = 2.15–2.64. Sample films were loaded by manually operating the screw. To maintain a uniform strain rate, the screw was turned as steadily and slowly as possible with a minute little twist of the fingers at a time. The average shear strain rate varied approximately from 3.3×10^{-5} to 4.08×10^{-5} s^{-1} within and between experimental runs. A small normal load applied with a pair of spring clips put a constraint on the sample film in the vertical direction. The bulk strain was heterogeneous and approximately in-plane.

INITIAL FABRIC

Different initial fabrics were generated by melting and hot-pressing the wax. In melt-grown films (Fig. 1c) sandwiched between two preheated ($T > T_m$) glass slides, uniform cooling produced a range (0.01–0.03 mm) of fine-grained, evenly crystalline, interlocking textures with curved and/or straight grain-boundaries. The resulting fabric comprised strain-free grains of near-random geometric and crystallographic orientations, except at the sample periphery where dimensionally oriented elongate grains defined a narrow domain of shape fabric. Less than 10% of the film-area in the isotropic parts, however, comprised small islands of fine-grained aggregates amidst relatively coarse-grained surrounding.

Hot-pressed films were generated pressing solid paraffin wax between two glass slides while the temperature was gradually raised to T_m. During crystallization under a nominal vertical load applied by the spring clips, small plates ($\leq$ 0.03 mm) of various shapes, triangular, rectangular, equant and polygonal, appeared first, followed by recrystallization of needles from plates. Both forms grew to a large size ($\leq$ 0.08 mm) under slow cooling. A range of initial grain-shape fabrics could be generated by heating only a limited area or a large area. With a limited area heat-source, such as a candle located below the glass-slides, a falling temperature gradient was established from the centre to the periphery of the sample films. Slow cooling started crystallization, leading to a flow layering comprising alternate domains of random and anisotropic fabric (Fig. 1d) of varying width toward the periphery, and an isotropic fabric in the central part of the thin film. In contrast, a pervasive anisotropy was developed with varying heat treatment ($T < T_m$) using a large area heat-source.

Intergranular gaps, grain-scale micro-cracks and minute air bubbles were present in most of the samples, irrespective of the technique followed. At elevated temperatures of 32–43°C, thermal volume expansion of air in air-tight cylindrical bubbles (with the circular cross-section lying in the sample plane) exerted an outward pressure. There was also an excess pressure on the bubble-wall due to the effects of surface tension. Effectively, this made the bubbles behave as deformable stiff inclusions in the strain- and temperature-softened matrix wax (discussed further in a later section).

RESULTS OF BRITTLE DEFORMATION

En échelon fracture arrays

The starting material for a brittle experiment was a melt-grown film with near-random geometric and crystallographic fabrics in most parts (as in Fig. 1c), and a peripheral narrow zone of primary grain-shape anisotropy oriented at a counterclockwise angle of 40–50° to the wall. Progressive brittle and brittle–ductile deformation of the films produced segmented fault zones (e.g. Fig. 5) comprising en échelon fracture arrays whose overall patterns were qualitatively similar in different experimental runs. The fracture arrays developed in the following order:

(a) early concomitant development of: (i) primary, RS (right-stepping), en échelon (tensile) T-fractures, T_1, at counterclockwise angles of 40–45° to the shear zone; and (ii) spaced cleavage, S_c, sub-perpendicular to T_1, in the anisotropic periphery close to one wall of the shear zone (Fig. 1e);

(b) early initiation and propagation of first-order, RS, LL (left-lateral), en échelon shear fractures at clockwise angles of 10–15° to the direction of shear; establishing fault segment F_1, diagonally across the shear zone (Figs.

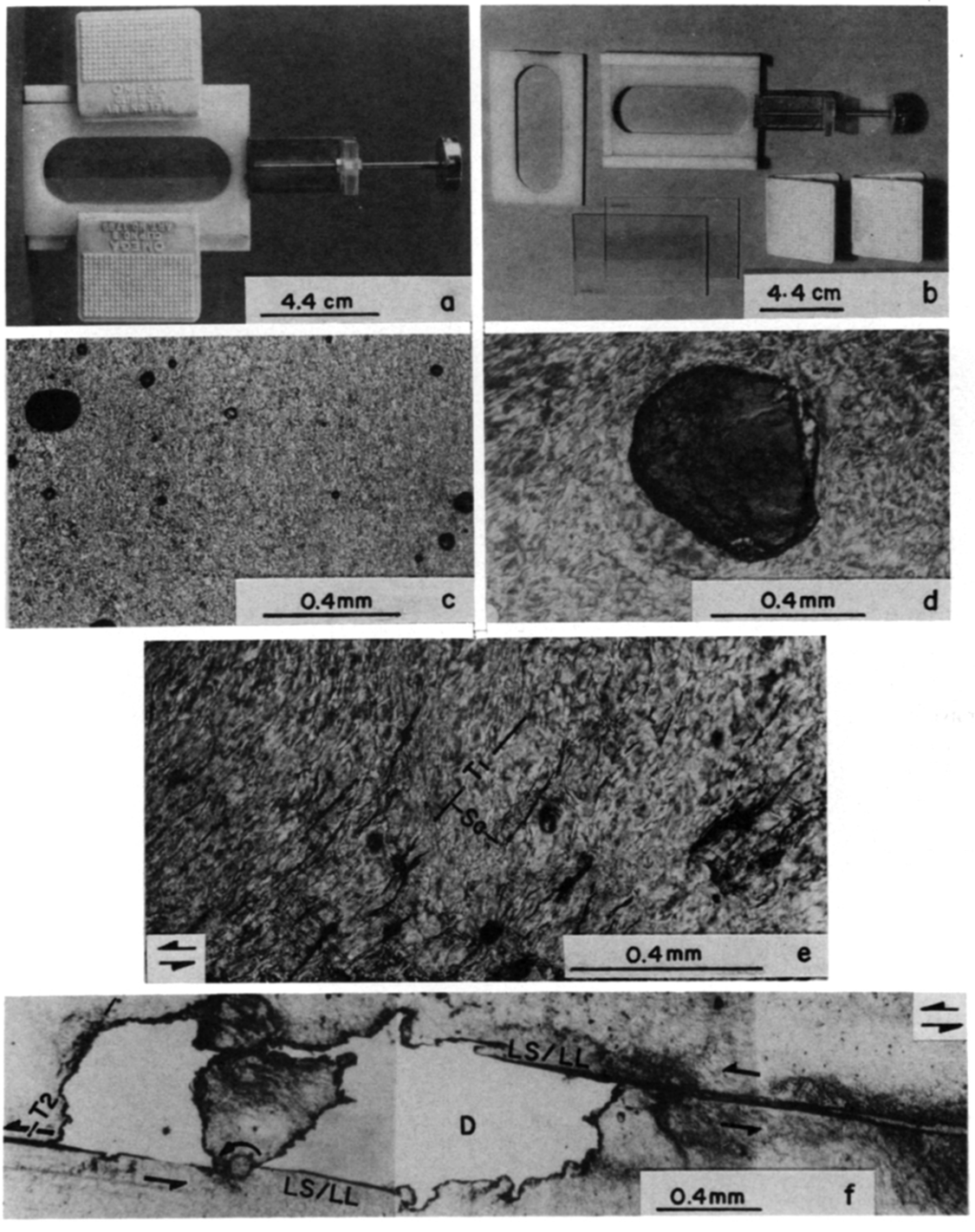

Fig. 1. (a) Apparatus assembly; (b) component parts; (c) melt-grown, near-random (dark spots are air bubbles); and (d) hot-pressed, anisotropic (large dark area is an air bubble) initial fabrics in transparent paraffin wax films. (e) Simultaneous development of primary T-fractures, T_1, and spaced cleavage, S_c, in the anisotropic periphery of a melt-grown film. (f) Second-order T-fractures, T_2, across a bridge between a pair of LS–LL shears in the isotropic part of the same film. Note the development of fabric adjacent to the shears and anticlockwise rotation of the irregular pod within a tailed, open gash, D (gashes here represent geometrical shapes of natural dominoes in tensile bridges of rock). Shear sense is top-to-the-left in (e) and (f), and in all subsequent figures.

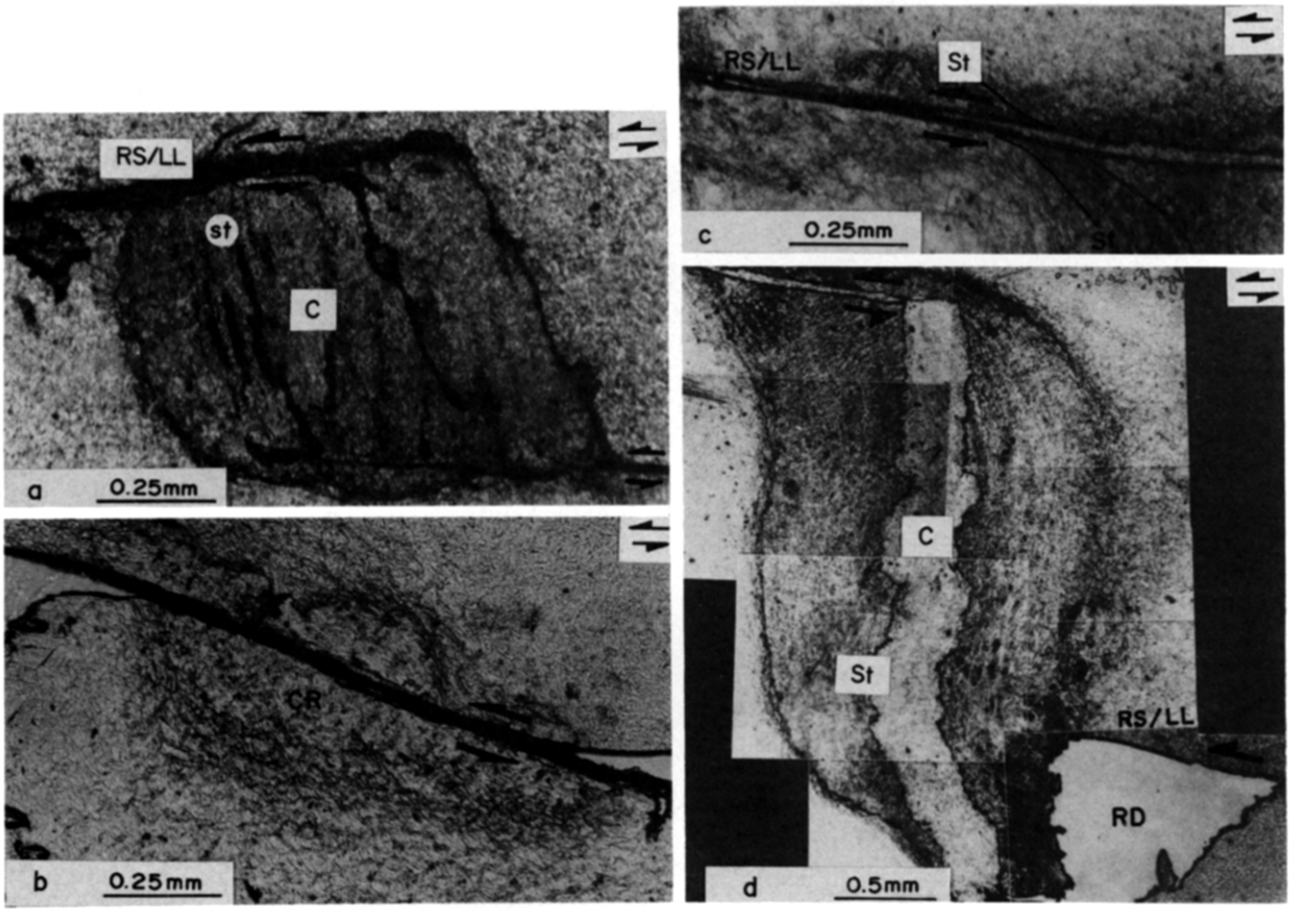

Fig. 2. Brittle and brittle–ductile structures developed in the central part of a melt-grown film with near-random initial fabric. (a) A compressive bridge (see Fig. 5, C) with S_t, between a pair of overlapping and deviated RS–LL shears. (b) A restraining bend of a LS–LL shear; deformation induced shape-fabric around the bend contrasts with the initial fabric in the northeast corner of the field. (c) Bent, dragged and offset S_t trails across a RS–LL shear. (d) Sigmoidal S_t trails within a compressive bridge (initial fabric is preserved in the northeast and southeast corners and along the left margin of the field); and RD, a rotated domino-shaped gash occurring in transition to a compressive bridge; note the initial fabric in the northeast corner.

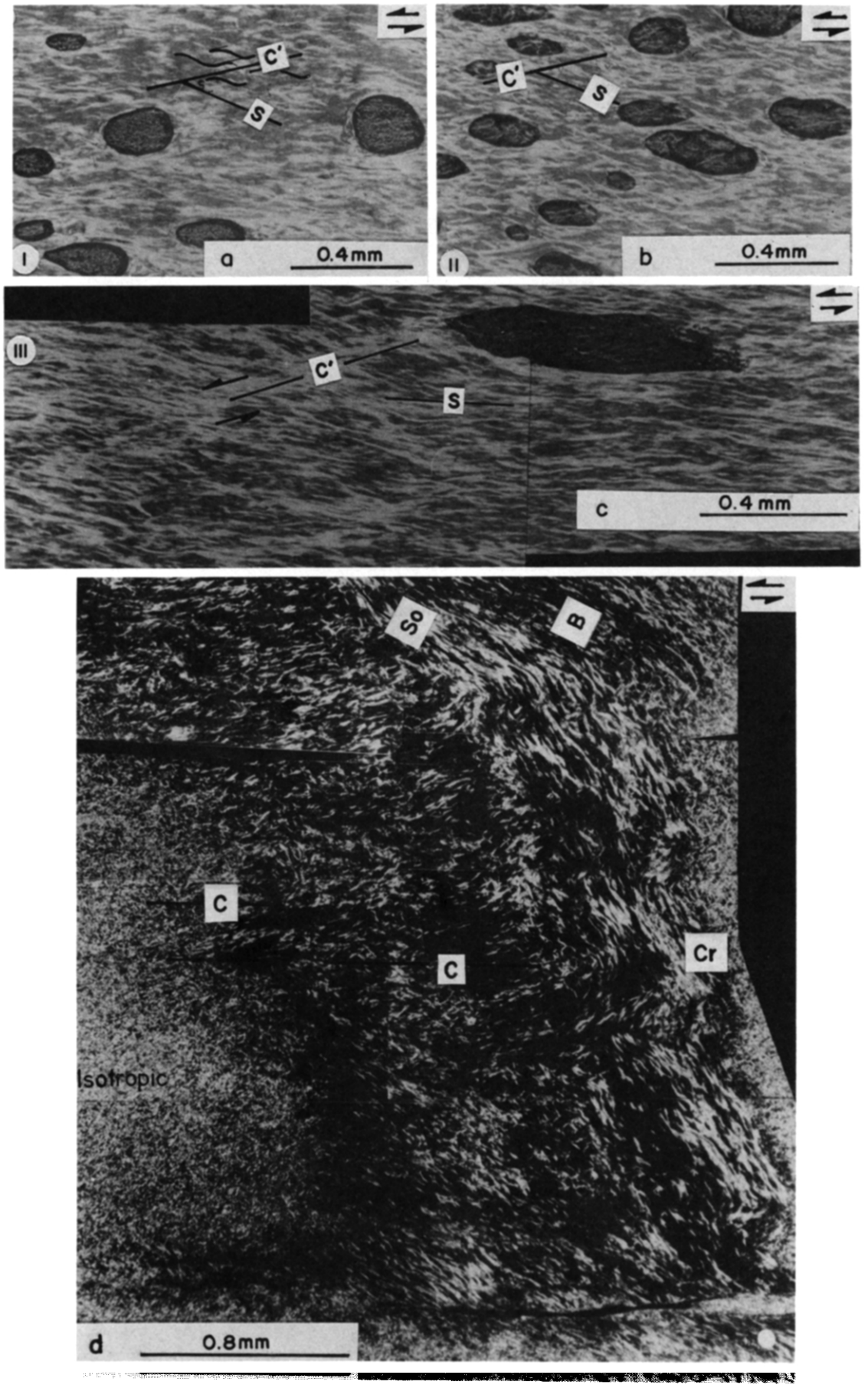

Fig. 3. Ductile microstructures developed in the isotropic central part of a hot-pressed film. (a) Simultaneous development of two foliations from an initial isotropic fabric; shear zone foliation, S, and discontinuous asymmetrical extensional shear bands, C', at stage I, $\gamma = 0.66$; (b) development at an intermediate stage II, $\gamma = 1.4$; and (c) continuous asymmetrical extensional shear bands with synthetic displacement of S along C' at a late stage III, $\gamma = 2.64$. Note the rotation of S with respect to C' and reduction in the average $C' \wedge S$ angle from 35° to 28°. (d) Crenulation, Cr, on primary S_0 in the anisotropic periphery of the same film, at $\gamma = 2.64$. Note: the isotropic surroundings (as in Fig. 1c) along the left and right margins of the field; discrete shear planes, C, and boudinaged long limbs, B. The plane of anisotropy was at a counterclockwise angle of 65° to the extension direction at the start of deformation.

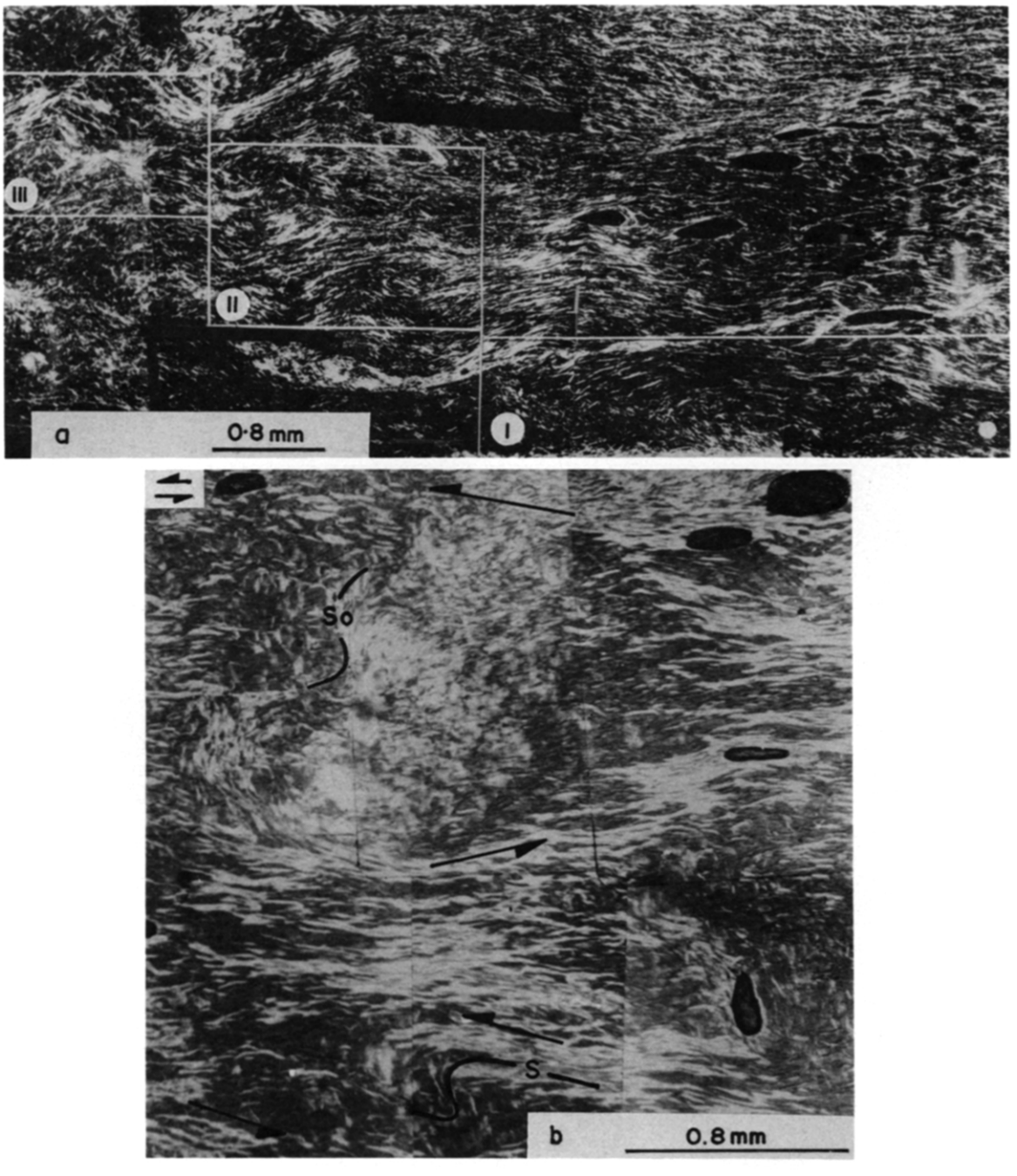

Fig. 4. Development of ductile structures in the same hot-pressed film shown in Fig. 3. (a) Photomicrographic mosaic of a segment of strain- and temperature-softened shear zone (at $\gamma = 2.64$) developed in the isotropic central part which has local S_0 oriented at 65–70° to the wall. Boxes I, II and III correspond, respectively, to folds of S with axial traces at low, moderate and high angles to the shear zone boundaries; note development of banding in the northeast corner (dark elliptical areas are deformed bubbles). (b) Shear lenses superimposed on pre-existing or early deformation fabrics by anastomosing shears; early folds of S_0 with 'S' asymmetry are preserved within the lenses (top and right margins). A late asymmetric fold within a lens is shown at the bottom left.

2a and 5 show deviated segments of a pair of overlapped RS–LL fractures near a compressive bridge);

(c) late propagation of first-order, LS (left-stepping), LL, en échelon shear fractures at clockwise angles of 10–15° to the direction of shear; producing fault segment F_2 (Figs. 1f and 5); and

(d) late development of second-order, RS, T-fractures, T_2, at counterclockwise angles of 50–55° to the shear zone boundary, across the bridges between first-order LS–LL fractures (Figs. 1f and 5).

Compressive bridges

Once a small overlap was established between a pair of propagating RS–LL shears in the F_1 segment, the approaching tips deviated from each other. With large overlap (Fig. 2a), propagation by shear was inhibited and eventually stopped when the tips approached each other in curved paths. Compressive bridges (C, Fig. 5) developed in the following areas:

(a) in the overlap between the adjacent tips of a pair of first-order, RS–LL shears (Fig. 2a); and

(b) around the restraining bends (CR in Figs. 2b and 5) of RS–LL shears.

Increasing strain produced a variety of microstructures, within the compressive bridges, around the restraining bends, and adjacent to the fractures, which include: (i) stylolite-like cleavage, S_t (Fig. 2a) across the bridges linking the first-order shears; (ii) a crystal-shape fabric (Fig. 2b); (iii) bent, dragged and off-set S_t trails across the shear fractures (Fig. 2c); and (iv) sigmoidal S_t trails (Fig. 2d).

Tensile bridges

With progressive shear, tensile bridges developed in the overlap between a pair of propagating LS–LL shears of fault segment F_2. Ordinary and tailed gashes, similar in geometrical shape to dominoes in tensile bridges of rock, developed by the opening of:

(a) T_2 across the bridges between the adjacent tips of a pair of LS–LL shears (D, Figs. 1f and 5);

(b) T_2 transected by a small transform fault, FF, within the bridges (DF, Fig. 5); and

(c) T_2 transitional to the rotated sigmoidal trails within compressive bridges (RD, Figs. 2d and 5).

RESULTS OF DUCTILE DEFORMATION

The starting material for a ductile experiment was a hot-pressed film with isotropic fabrics in the central part, and alternate random and anisotropic fabric-domains towards the periphery. The anisotropic plane made a counterclockwise angle of 65–75° to the shear zone at the start of deformation. During experimental runs, narrow and anastomosing shear zones of finite width and length developed with deformation microstructures in the isotropic parts somewhat different from those in the anisotropic parts. The variety of non-pervasive, micro- and meso-scale structures produced in different parts of the shear zone includes the following.

C′–S fabrics

With accumulation of finite strain, two sets of discontinuous shape fabrics, asymmetrical extensional shear bands, C', and foliation, S, developed simultaneously in the isotropic central part of the sample film. At a certain stage I ($\gamma = 0.66$), S was oriented at an average clockwise angle of 20°, and sporadic normal slip crenulations and/or a crenulation foliation defining C' developed at a counterclockwise angle of 15° to the direction of shear (Fig. 3a), making an average $C' \wedge S$ angle of 35°. With progressive simple shear, the $C' \wedge S$ angle gradually reduced to 28° (stages II–III, Figs. 3b & c). At $\gamma = 2.15$–2.64, discontinuous and sporadic C' matured into narrow and continuous shear bands offsetting S in a synthetic (LL) sense. With increasing strain, crystallographic realignment of grains along C' and S planes led to a progressive change of compensation colours from red → yellow → green.

The aspect ratio and the long axis orientation of differently sized elliptical (in two dimensions) bubbles enclosed within the foliated matrix were variable (between 1.6 and 2 in Stage I, 2.75–3.6 in Stage II and 5–6 in Stage III) at any given stage of deformation.

Asymmetric tails

With progressive deformation, asymmetric tail structures and pressure shadows developed around the air bubbles and the platy crystals. They had the following geometry:

(a) matrix foliation asymmetrically wrapped around elliptical air bubbles and aggregates of platy crystals (Fig. 3a);

(b) σ- and δ-type asymmetric 'tails' with stair-stepping geometry around differently sized elliptical air bubbles of varying orientations (Figs. 3a & b and 6); and

(c) sigmoidal tails of foliation bent along the asymmetrical extensional shear bands (Fig. 3c).

Early folds of pre-existing anisotropy

Pre-existing planar anisotropy, S_0, initially oriented at counterclockwise angles of 65–70° to the shear direction, was crenulated (Cr) and rotated in the same sense as the bulk simple shear (Fig. 3d) with progressive deformation. The axial planes of the crenulations were oriented at low clockwise angles to the shear zone early during active, stable folding. As deformation progressed, folding followed by stretching produced asymmetric, unstable crenulations with boudinaged long limbs, B, (Fig. 3d). Although deformation was fairly constant along the shear zone, the effects of deformation were different in different parts because of variation in the initial fabrics, and in their mechanical anisotropy. Near the periphery, visible effects of deformation were

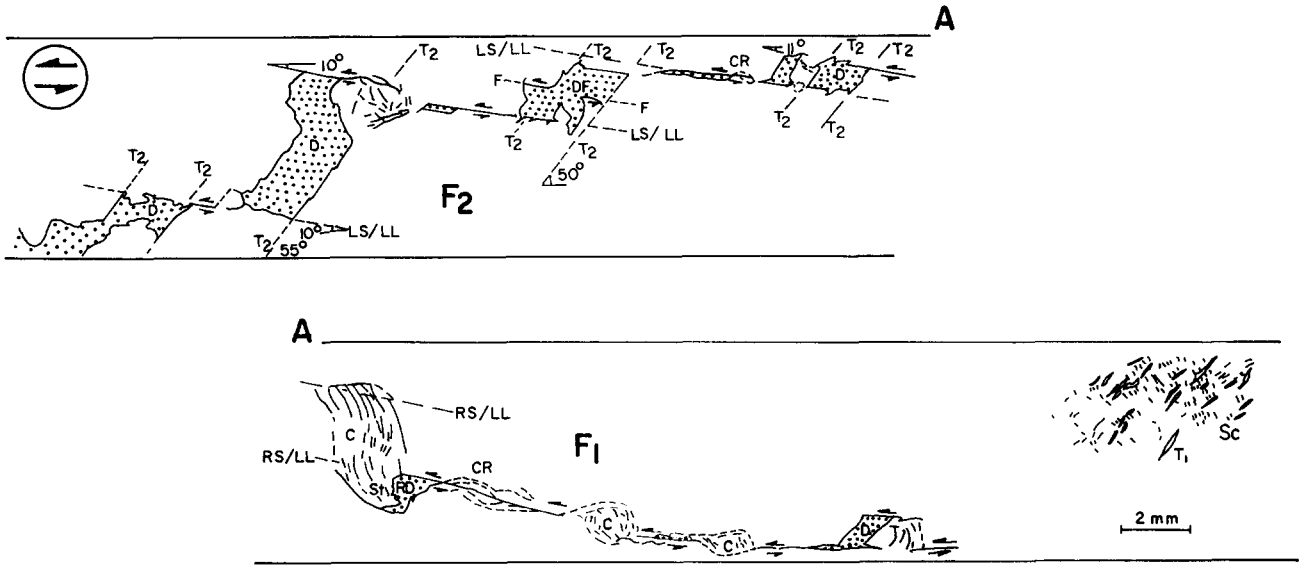

Fig. 5. RS–LL and LS–LL en échelon fracture arrays of fault segments F_1 and F_2, respectively. RS–LL, early first-order shears, deviated when overlapping near compressive bridges, C; S_1, stylolitic cleavage (fine lines) within C; LS–LL, late first-order shears; T_2, late second-order tensile fractures; D, tailed and ordinary, domino-shaped open gashes (stippled area); FF, a transform fault across a domino-like gash; RD, a rotated domino-like gash, although characteristic of a tensile bridge, occurs in transition to a compressive bridge; CR, transpressive restraining bends of RS and LS shears; T_1, primary tensile fracture; and S_c, spaced cleavage.

more pronounced (open to chevron fold geometry) in the anisotropic planes than in the immediate isotropic surrounding. Traces of the folded form surfaces on the sample plane (XZ_f) revealed that within the plane of anisotropy itself, thin laminae were more appressed than thick laminae. The orientation of the fold axes with respect to the Y direction could not be determined from two dimensional observation. With progressive rotation towards the bulk flow plane, the axial planes of the crenulations became active as discrete slip surfaces, C. The microstructures within the anisotropic domain resembled C–S fabrics (Fig. 7) at this stage of deformation ($\gamma = 2.64$).

Late folds in shear zone foliation

With progressive shearing, stable and unstable active folds developed discontinuously in shear zone foliation, S, and pre-existing anisotropy, S_0. Late during deformation, local deflections of S were amplified into stable asymmetric folds with vergence the same as for the bulk simple shear, while early folds in S_0 with an initial 'S' asymmetry were stretched and boudinaged into unstable folds with 'Z' asymmetry. Traces of the folded S surfaces on the XZ_f plane assumed the following forms and geometry (Fig. 4a, Boxes I, II and III, respectively):

(a) open, chevron to tight (interlimb angle *ca* 30°) folds with axial traces at moderate to low clockwise angles to the shear direction (Fig. 8a):

(b) open, asymmetric disharmonic folds with axial traces at low to moderate angles to the shear zone walls (Fig. 8b); and

(c) open, symmetric disharmonic folds with axial traces at high angles to the shear zone walls (Fig. 8c).

Shear lenses

Lenses and pods comprising deformed aggregates of platy crystals developed in successive stages during inhomogeneous deformation. Superimposition of narrow zones of highly localized shear-strain (characterized by highly elongate grains undergoing progressive change in compensation colours due to preferred crystallographic realignment) at various angles to the early formed deformation fabrics or pre-existing primary fabrics led to the following cases of lens development:

(a) the width of the bounding shears increased, gradually deforming while enclosing the adjoining pods and lenses partly or completely, with superimposition of a late foliation at a clockwise acute angle to the enveloping shears (Fig. 4b);

(b) early microfolds in S_0 with 'S' asymmetry remained preserved within the relatively less deformed lenses, while the newly superimposed foliation developed sub-parallel to the enveloping shears (top left, Figs. 4b and 9); and

(c) asymmetric microfolds developed in the early shear zone foliation, S, within the lenses, while the newly superimposed foliation developed axial planar to the folds (bottom left, Figs. 4b and 9).

DISCUSSION

Structures produced in the brittle experiments are analogous to those of certain shallow-level fault zones comprising en échelon fracture arrays, compressive and tensile bridges and other within-bridge microstructures (Gammond 1983, 1987). Concomitant development of T_1 and S_c in the periphery is indicative of a local brittle–

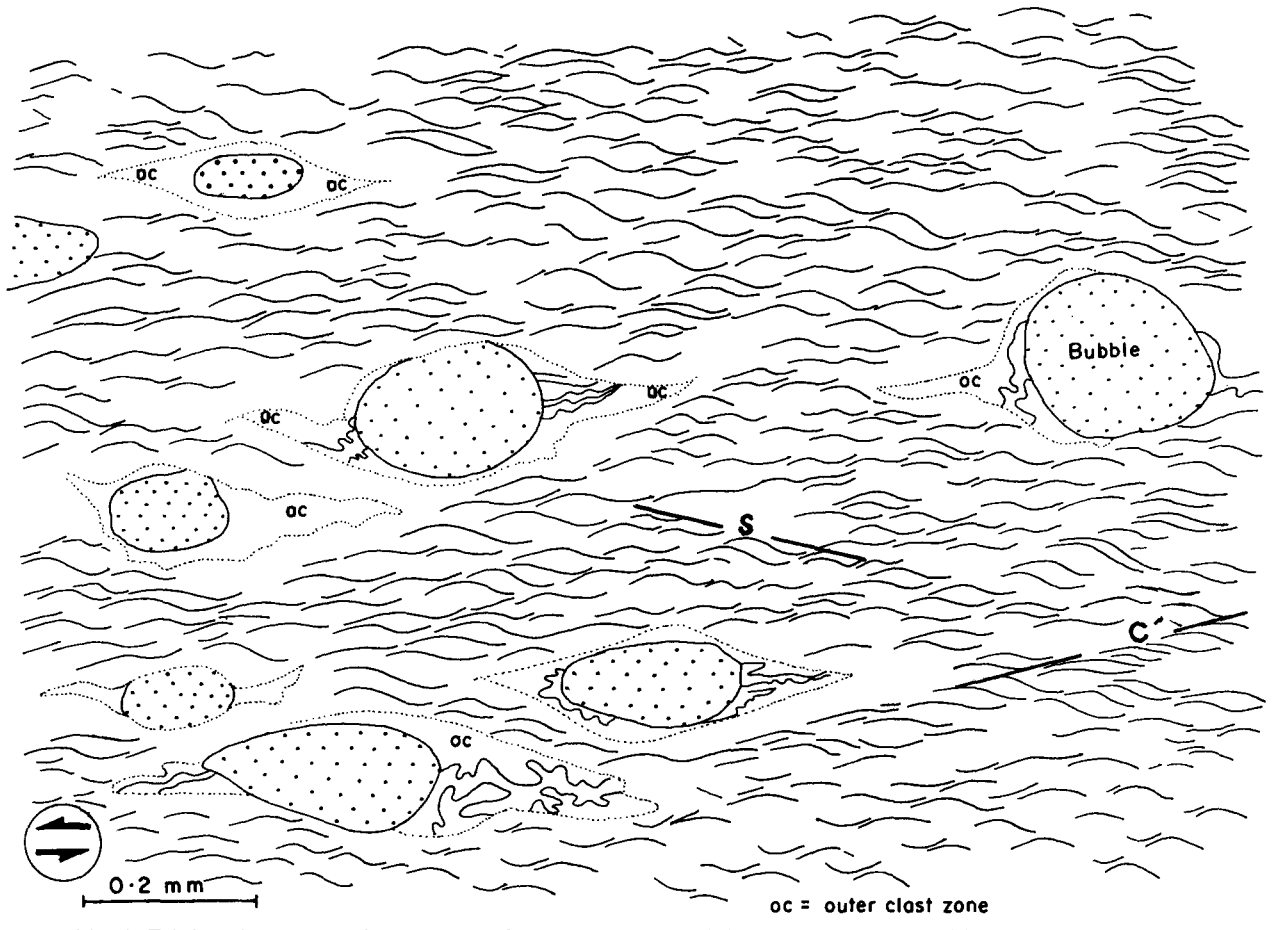

Fig. 6. Fabric trajectory map showing σ- and δ-type wings around air bubbles shown in Fig. 3(a). The stippled areas are bubbles.

ductile strain which is factored into heterogeneous simple shear and a small positive dilatation resulting in a wall-normal strain.

The observed orientations of T_1 and S_c are related, consistent with Ramsay & Huber (1983, p. 42), to the principal stretch axes of the finite strain ellipse. Pre-existing anisotropy normal to the maximum stretching axis of the finite strain ellipse controls development of T_1 in the sample periphery.

With the initial accumulation of finite strain, an incipient fabric develops in response to a combination of processes which include interlinking of branched microcracks, collapse of intergranular space, grain comminution, grain rotation, grain-boundary sliding and grain flattening. Initiation and orientation of the RS–LL shears are largely controlled by this syn-deformational fabric. The RS–LL shears continue to propagate until accumulated wall-normal strain resulting from the tractive motion is large enough to stop their further propagation (Gammond 1983). Other effects of wall-normal strain are material-hardening within the shear zone due to which the development of T_1 and S_c is strongly inhibited, and inducement of more fabric anisotropy. Further extension of the shear zone now takes place by the reactivation of these deformation-fabrics leading to LS–LL fracturing under shear.

The development of LS–LL shears as first-generation arrays is consistent with Gammond (1987), and suggests that they need not necessarily initiate as second-order fractures by stress-reorientation within the compressive bridges, as proposed by Morgenstern & Tchalenko (1967).

The controlling factors in the segmented development of a fault zone under simple shear are the boundary conditions, the extent to which the shear zone material can accommodate wall-normal strain, favourable orientation of the pre- or syn-deformational anisotropy, and the sense of stepping of early formed fracture arrays. Under the present boundary conditions, the development initiates with T_1 fracturing, passes through RS–LL shearing, and culminates in LS–LL shearing and T_2 fracturing.

Stress reorientations, as proposed by Segall & Pollard (1980), are important for the development of within-bridge micro-structures such as sigmoidal S_t trails, and ordinary and tailed dominoes. The present experiments, however, demonstrate that progressive reorientation of the principal stretch axes of a pre-existing strain ellipse with a superimposed incremental strain ellipse may also lead to their development. It is interesting to note that both compressive and tensile bridges may result from the interaction of overlapping LL shears in the segmented sinistral fault zone.

The deformation microfabrics and structures produced in the ductile experiments strongly resemble natural examples. S develops as a strain-sensitive,

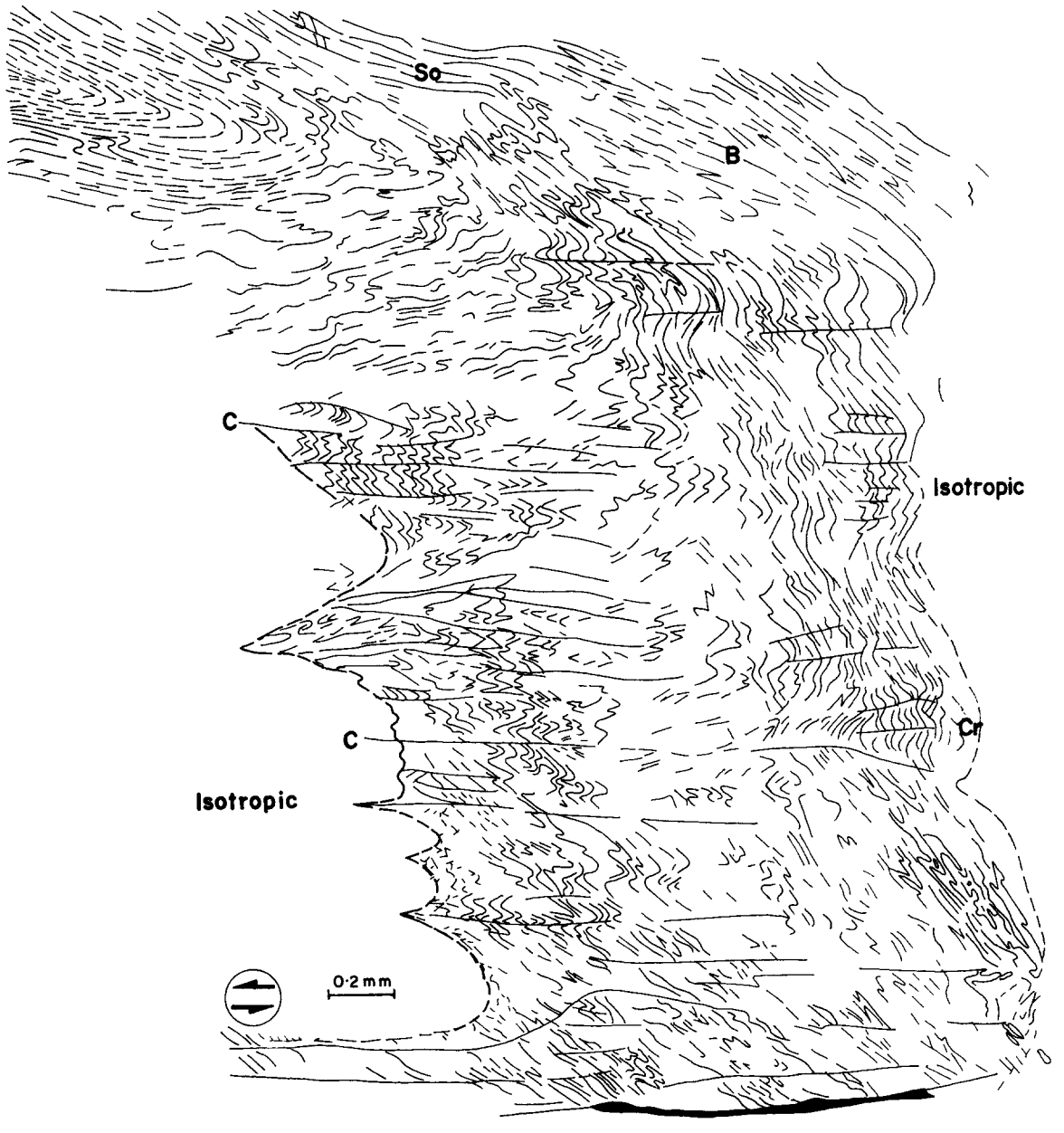

Fig. 7. Fabric trajectory map of Fig. 3(d); shortening of S_0 followed by stretching has produced boudinaged folds in the planar anisotropic fabric; depending on the thickness of the individual laminae, folds are chevron to open; *C–S* fabrics have developed at $\gamma = 2.15$–2.64.

microscopically visible fabric at and above $\gamma = 0.66$, and closely tracks the XY_f plane, consistent with Ramsay (1980) and Ghosh (1982). Matching of the long axis trajectories of the elliptical bubbles with the fabric trajectories (Fig. 3a), however, implies different net rotation of the bubble-enclosing matrix foliation at different places within the shear zone. This is possible if *S* is back-rotated during progressive shearing.

Discontinuous development of *C'*, simultaneously with *S*, is related to slip along *S* planes, in accord with Dennis & Secor (1987). *C'* planes develop to accommodate components of foliation slip normal to the overall movement direction in the shear zone between the rigid walls. This requires local yielding along *S*, early during deformation ($\gamma = 0.66$) for *C'* to form (Lister & Snoke 1984), and back-rotation of *S* in the microlithon between any two *C'* planes. With initiation of material softening and localization of relatively high strain ($\gamma = 2.64$), *C'* develops into continuous asymmetrical extensional shear bands. The decrease in $C' \wedge S$ angle from 35° to 28° with increasing strain is consistent with Berthé *et al.* (1979), although the angular relationships between the two simulated fabrics (*C'–S*) show lower values as a function of progressive shear strain, probably due to the different rheological behaviour of paraffin wax.

The modelled *C'–S* fabrics (nomenclature after Hanmer & Passchier 1991) being strain sensitive, do not appear to have formed in a manner suggested by White *et al.* (1980) for this type of microstructure, because neither the temperature nor the shear direction changes

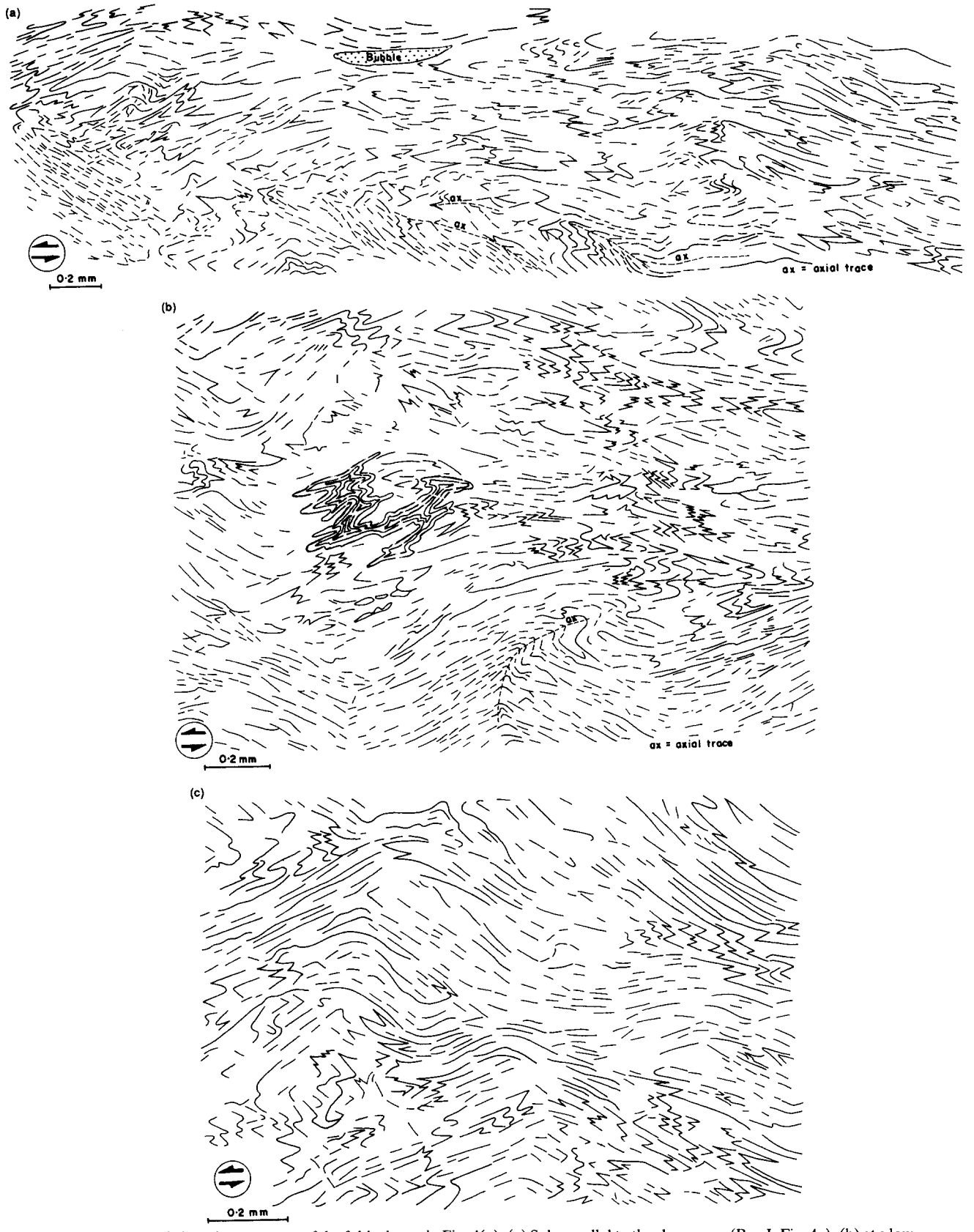

Fig. 8. Fabric trajectory maps of the folds shown in Fig. 4(a). (a) Sub-parallel to the shear zone (Box I, Fig. 4a); (b) at a low angle to the shear zone (Box II); and (c) at a high angle to the zone boundary (Box III). The stippled elliptical areas are bubbles.

during the deformation, nor is there strain hardening or strain-rate hardening associated with *S*. *S* is active throughout the deformation (shown by gradual change in compensation colours with progressive crystallographic realignment, Fig. 3c). This is consistent with Vernon *et al.* (1983) who suggested that both *S* and *C* participate actively in accommodating strain during mylonitization of rock. Interestingly, in the present

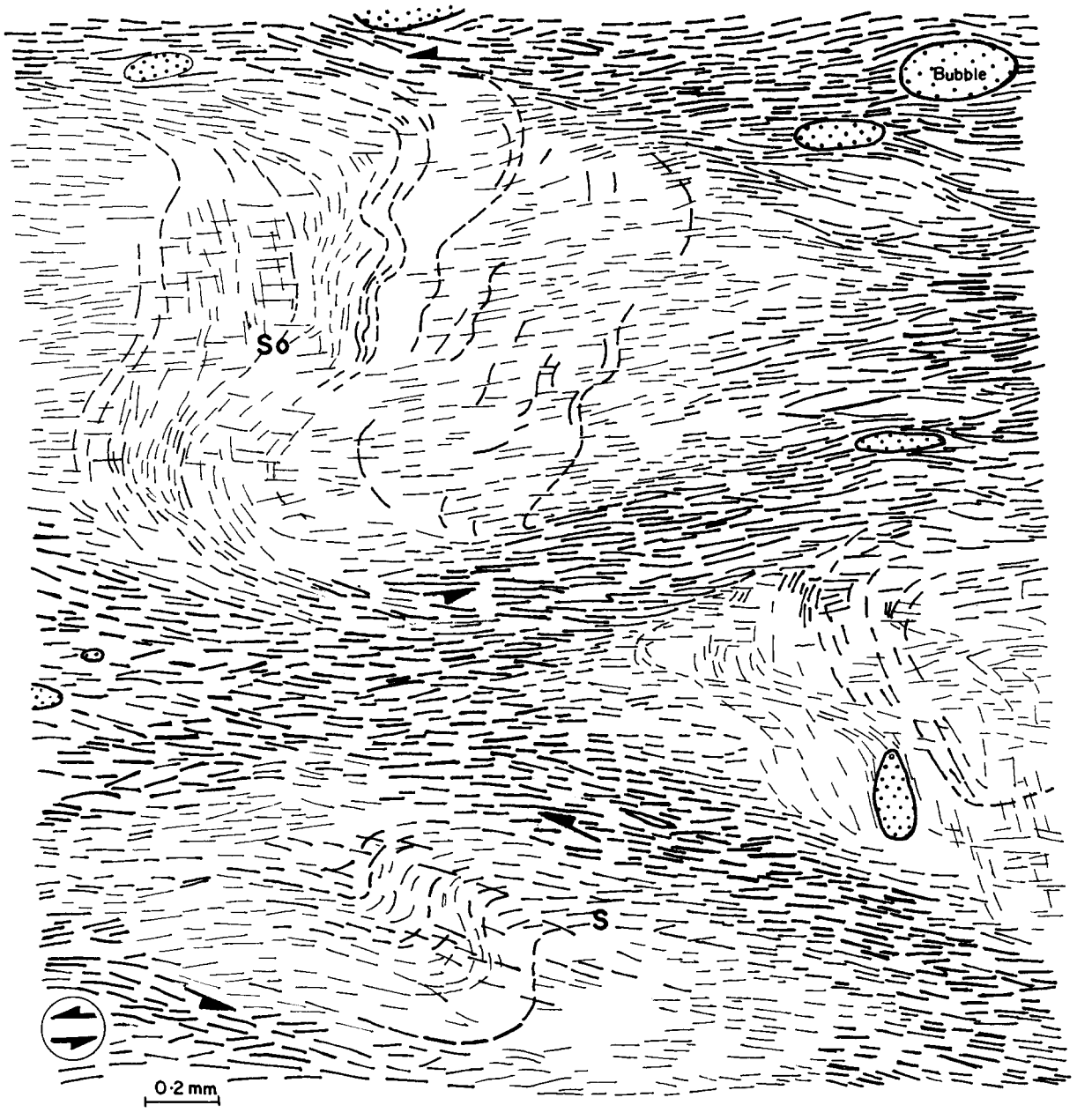

Fig. 9. Details of fabric and microstructural development within the superimposed shear lenses shown in Fig. 4(b). Top left—early folds in S_0 with 'S' asymmetry, and stretched limbs in the enveloping LL shears. Bottom left—superimposition of a shear lens on early foliation, S. An asymmetric fold develops when S is at a counterclockwise acute angle to the bounding shears. The newly developed foliation is axial planar to the early folds; the stippled areas are bubbles.

models, it is the asymmetrical extensional shear bands, C', rather than shear-zone parallel C bands, which form with progressive non-coaxial deformation.

Asymmetric pressure shadows and straight and folded asymmetric tails (e.g. winged porphyroclasts and winged inclusions), have been studied in detail by several workers (Ghosh & Ramberg 1976, Hanmer 1986, Passchier & Simpson 1986, Passchier 1987, Van Den Driessche & Brun 1987). Present observations (Figs. 3a & b) on asymmetric tails are in conformity, in many aspects, with the previous work. The modelled clasts (air bubbles) in the σ- and δ-structures, although in a sense stiffer than wax, cannot be said to rotate as rigid porphyroclasts. They rotate with the enclosing matrix foliation, S, under the influence of shear, and differ in orientation because of different amounts of back-rotation of S between the adjacent C' planes.

As progressive deformation changes circular cross sections of the bubbles to elliptical shapes of increasing aspect ratio, the wall curvature of the bubbles becomes decreasingly lower in the two shortening quadrants and increasingly higher in the two extensional quadrants. Effects of surface tension and curvature controlled mass transfer will tend to restore the bubbles to a circular shape, in accordance with Hudleston (1977, p. 140). This effect is stronger for small bubbles than for large ones.

If there are local C' planes in the immediate vicinity of the two high curvature ends of an elliptical bubble, then wax diffusing or flowing into these ends from the low

curvature regions may be drawn out along the C' planes away from the bubble in a manner analogous to that proposed by Passchier & Simpson (1986) for σ- and δ-type wing structures. One significant difference is that the wings in my models are matrix derived. Given the variable aspect ratios of differently sized bubbles and their different orientations, either σ or δ structure may form in accordance with Simpson & De Paor (1993). Asymmetrical tails associated with rigid and semi-rigid, elliptical plates of wax have formed, on the other hand, by deflection and flow of S around these bodies, or by sigmoidal deflection and flow of foliation along asymmetrical extensional shear bands, C' (Figs. 3a–c; details in Fig. 6).

Stable and unstable active folding of a pre-existing planar anisotropy whose mechanical properties are different from the isotropic surrounding, as in this case, is a common consequence of progressive deformation. Oblique anisotropy planes are initially shortened by buckling and later stretched, in accordance with Ramsay & Huber (1983, p. 224), producing crenulated short limbs and boudinaged long limbs (Fig. 3d). The modifications are the result of oblique orientation of the principal incremental strains with respect to the pre-existing anisotropy. Rotation of the axial planes of the crenulations towards the flow plane and their eventual development into discrete, shear-parallel slip surfaces, C, across S_0 (Fig. 7), implies strain hardening of deformed fabrics within the anisotropic domains at the periphery of the model.

Development of discontinuous folds in an essentially stretching fabric, S, has been explained by Lister & Williams (1983), Platt (1983) and Ghosh & Sengupta (1987). Figures 8(a)–(c) are the respective fabric trajectory maps showing the details of stable folding of the developing foliation, S, and unstable folding of the pre-existing anisotropy, S_0. Factors controlling such developments are: (a) the spatial variation in the mechanical anisotropy of early and late deformation fabrics, due to which foliation-parallel slip is facilitated at one place while inhibited at others, resulting in layer-parallel shortening; (b) the presence of bubbles and platy crystals in the flow field of wax, around which foliation is deflected and the deflection is amplified by progressive shear; and (c) the asperities on the edges of the frosted grips around which perturbations grow with progressive deformation.

Total displacement in the modelled shear zones has been achieved by separate displacements along small shears around the lenses, producing anastomosing patterns (Fig. 4b), in a manner similar to the coalescence of primary and secondary shears suggested by Tchalenko (1968, 1970). In some parts, however, approach and intersection of two narrow zones of high strain (Fig. 4a) appears to have developed shear lenses, in accordance with Ramsay (1980).

As the bounding shears widen with progressive deformation, they superimpose on the pre-existing fabrics a new foliation at a clockwise acute angle to the local shear direction. Within some lenses (as in Fig. 9, top left), the new foliation develops axial planar to the early folds in S_0. Where at a counterclockwise acute angle to the superimposed shears (as in Fig. 9, bottom left), the early S planes lying in the shortening quadrants are asymmetrically folded with the newly superimposed foliation developing axial planar to the folds.

CONCLUSIONS

The experiments help to demonstrate the following.

(a) Even in a single isotropic medium undergoing sinistral simple shear, a segmented fault zone may develop with RS–LL and LS–LL primary fracture arrays constituting the separate segments. Rigid boundary conditions and reactivation of fabric anisotropy control the order and extent of such a development.

(b) Both compressive and tensile bridges may develop with fracture arrays of the same generation and displacement sense, depending on their sense of stepping and degree of overlap.

(c) In a sinistral fault zone, within-bridge microstructures may develop perpendicular to maximum shortening or maximum extension and may gradually rotate in a clockwise or anticlockwise sense, as the case may be, depending on whether the bridge is compressive or tensile.

(d) In a shear zone, the induced foliation closely tracks the XY plane of finite strain, but its development as a microfabric only becomes perceptible by the time the finite strain ellipse has rotated by a finite angle (25° in this case) towards the bulk flow plane.

(e) In a ductile shear zone of constant width, C' and S planar fabrics may develop simultaneously from an isotropic material undergoing heterogeneous simple shear. C' develops to accommodate the wall-normal component of foliation-parallel slip.

(f) σ and δ wings may form around bubbles or plates of wax if the particles have different aspect ratio and different orientation.

(g) Spatial differences in the mechanical inhomogeneity associated with the pre-existing and transposed layering, in the mechanical strength anisotropy of individual crystals of a single monomineralic phase, in the angular relationships between pre-existing fabrics and the shear direction, and in the heterogeneous strain are some experimentally valid factors that initiate internal buckle folds in a shear zone.

(h) It is possible to simulate brittle and ductile deformation processes leading to generation of micro- and meso-scale kinematic structures in a single material using the same experimental technique.

Acknowledgements—This research was encouraged by B. C. Poddar, Deputy Director General, Geological Survey of India, Central Region. I am particularly thankful to P. J. Hudleston, J. Van Den Driessche and an anonymous reviewer for their critical comments in improving the manuscript. I thank S. K. Ray and B. K. Chakraborty for helpful discussion in preparing the early manuscript and K. Muthuraman and Mohd. Iqbal for assistance with word processing. I also thank Mukta Chatterjee for encouragement at home.

REFERENCES

Berthé, D. & Brun, J. P. 1980. Evolution of folds during progressive shear in the South Armorican shear zone, France. *J. Struct. Geol.* **2**, 127–133.

Berthé, D., Choukroune, P. & Jegouzo, P. 1979. Orthogneiss, mylonite and non-coaxial deformation of granite: the example of the South Armorican shear Zone. *J. Struct. Geol.* **1**, 31–42.

Casas, J. M. 1986. Shear-bands and related extensional structures in a mylonitized quartz-dyke. *J. Struct. Geol.* **8**, 693–699.

Dennis, A. J. & Secor, D. T. 1987. A model for development of crenulations in shear zones with applications from the Southern Appalachian Piedmont. *J. Struct. Geol.* **9**, 809–817.

Dunstan, A. E., Nash, A. W., Brooks, T. B. & Tizard, H. 1938. *The Science of Petroleum. Volume III*, 1941–1944. Oxford University Press, Oxford.

Gammond, J. F. 1983. Displacement features associated with fault-zones: a comparison between observed examples and experimental models. *J. Struct. Geol.* **5**, 33–45.

Gammond, J. F. 1987. Bridge structures as a sense of displacement criteria in fault-zones. *J. Struct. Geol.* **9**, 609–620.

Ghosh, S. K. 1982. The problem of shearing along axial plane foliation. *J. Struct. Geol.* **4**, 63–67.

Ghosh, S. K. & Ramberg, H. 1976. Reorientation of inclusions by a combination of pure shear and simple shear. *Tectonophysics* **34**, 1–70.

Ghosh, S. K. & Sengupta, S. 1987. Progressive development of structures in a ductile shear zone. *J. Struct. Geol.* **9**, 277–287.

Hancock, P. L. 1985. Brittle microtectonics: principles and practices. *J. Struct. Geol.* **7**, 437–457.

Hanmer, S, 1986. Asymmetrical pull-aparts and foliation fish as kinematic indicators. *J. Struct. Geol.* **8**, 111–122.

Hanmer, S. & Passchier, C. W. 1991. Shear-sense indicators. *Geol. Surv. Pap. Can.* **90-17**.

Hobbs, B. E., Means, W. D. & Williams, P. F. 1982. The relationship between foliation and strain: an experimental investigation. *J. Struct. Geol.* **4**, 411–428.

Hudleston, P. J. 1977. Progressive deformation and development of fabric across zones of shear in glacial ice. In: *Energetics of Geological Processes* (edited by Saxena, S. K. & Bhattacharji, S.). Springer, New York, 121–150.

Jacoby, W. R. 1976. Paraffin model experiment of plate tectonics. *Tectonophysics* **35**, 103–113.

Lister, G. S. & Snoke, A. W. 1984. *S–C* mylonites. *J. Struct. Geol.* **6**, 617–638.

Lister, G. S. & Williams, P. F. 1979. Fabric development in shear zones: theoretical controls and observed phenomena. *J. Struct. Geol.* **4**, 283–398.

Lister, G. S. & Williams, P. F. 1983. The partitioning of deformation in flowing rock masses. *Tectonophysics* **92**, 1–33.

Means, W. D. 1989. Synkinematic microscopy of transparent polycrystals. *J. Struct. Geol.* **11**, 163–174.

Means, W. D. & Xia, Z. G. 1981. Deformation of crystalline materials in thin sections. *Geology* **9**, 538–543.

Morgenstern, N. R. & Tchalenko, J. S. 1967. Microscopic structures in kaoline subjected to direct shear. *Geotechnique* **17**, 309–328.

Neurath, C. & Smith, R. B. 1982. The effect of material properties on growth rates of folding and boudinaged experiments with wax models. *J. Struct. Geol.* **4**, 215–229.

Passchier, C. W. 1987. Stable positions of rigid objects in non-coaxial flow—a study in vorticity analysis. *J. Struct. Geol.* **9**, 679–690.

Passchier, C. W. & Simpson, C. 1986. Porphyroclast systems as kinematic indicators. *J. Struct. Geol.* **12**, 831–844.

Platt, J. P. 1983. Progressive refolding in ductile shear zones. *J. Struct. Geol.* **5**, 619–622.

Petit, J. P. 1987. Criteria for the sense of movement on fault-surfaces in brittle rocks. *J. Struct. Geol.* **9**, 597–608.

Ramsay, J. G. 1980. Shear-zone geometry: a review. *J. Struct. Geol.* **2**, 83–99.

Ramsay, J. G. & Huber, M. I. 1983. *The Techniques of Modern Structural Geology*, Volume 1; *Strain Analysis*. Academic Press, London.

Segall, P. & Pollard, D. D. 1980. Mechanics of discontinuous faults. *J. geophys. Res.* **85**, 4337–4350.

Simpson, C. 1983. Strain and shape fabric variation associated with ductile shear zones. *J. Struct. Geol.* **5**, 61–72.

Simpson, C. & De Paor, D. G. 1993. Strain and kinematic analysis in general shear zones. *J. Struct. Geol.* **15**, 1–20.

Tchalenko, J. S. 1968. The evolution of kink bands and the development of compression textures in sheared clays. *Tectonophysics* **6**, 159–174.

Tchalenko, J. S. 1970. Similarities between shear zones of different magnitudes. *Bull. geol. Soc. Am.* **81**, 1625–1639.

Van Den Driessche, J. & Brun, J. P. 1987. Rolling structures at large shear strains. *J. Struct. Geol.* **9**, 691–704.

Vernon, R. H., Williams, V. A. & D'Arcy, W. F. 1983. Grain size reduction and foliation development in a deformed granite batholith. *Tectonophysics* **92**, 123–146.

White, S. H., Burrows, S. E., Carreras, J., Shaw, N. D. & Humphreys, F. J. 1980. On mylonite in ductile shear zones. *J. Struct. Geol.* **2**, 175–187.

Wilson, C. J. L. 1984. Shear-bands, crenulations and differentiated layering in ice–mica model. *J. Struct. Geol.* **6**, 303–320.